ADAPTIVE ACQUISITION TECHNIQUES FOR PLANAR NEAR-FIELD ANTENNA MEASUREMENTS

Daniël Janse van Rensburg
Nearfield Systems Inc.
19730 Magellan Drive,
Torrance, CA 90502-1104, USA

Derek McNamara & Garrett Parsons
University of Ottawa
800 King Edward Ave.,
Ottawa, ON K1N 6N5, Canada

ABSTRACT

The use of adaptive acquisition techniques to reduce the overall test time in planar near-field antenna measurements is described. A decision function is used to track the accuracy of a measurement as the data acquisition proceeds, and to halt such acquisition when this is considered sufficient for the measured quantity of importance. Possible decision functions are defined and compared. Several test cases are presented to show that significant test time reduction is possible when compared to traditional acquisition schemes.

Keywords: Antenna measurements, planar near-field, adaptive.

1.0 Introduction

As antenna performance complexity increases, so too does the suite of measurements that are needed to confirm whether a given antenna satisfies the required performance. Such more elaborate testing at once implies that these measurements will be more time-consuming. It is important to realize that it is not only the speed with which electronic instrumentation is able to operate that is of concern but also the acquisition time related to the three-dimensional movement of the antenna under test (AUT), or the acquisition probe. It is believed by many that "in developing products and systems, testing, and not design, is usually the more expensive, time-consuming, and difficult activity" [1]. In this paper we investigate a straightforward approach to reduce the data capture burden in planar near-field (PNF) measurements [2]. Two acquisition schemes are proposed and compared to the traditional[1] acquisition process. Both proposed acquisition schemes rely on the processing of the measured data during the measurement process to assess far-field data uncertainty and determine a suitable point of acquisition termination. The second of the two newly proposed techniques also adapts the near-field acquisition based on sampled data and is therefore an adaptive acquisition scheme. Typical test time reductions possible with these new acquisition techniques are presented.

Since the reduction of PNF data sets during acquisition is opposed by an ever increasing truncation impact, Section 2 contains a review of the methods that have been developed to help counter truncation. The acquisition schemes presented here, although affected by truncation, do not attempt to counter the effect of truncation and merely assesses the impact of the near-field boundary on the far-field result. The two new acquisition schemes are detailed in Section 3. The two decision functions employed in this paper are presented formally in Section 4 and Section 5 contains typical test time reductions that are achievable using the acquisition schemes proposed by comparing results to that obtained using the traditional acquisition process. Some conclusions are presented in Section 6.

2.0 Review of PNF Truncation Compensation Techniques

There is a well-established body of literature (for example [2], and references therein) on both the theoretical and practical aspects of PNF measurements. The electromagnetic theory upon which the PNF technique is based requires the measurement area to be an infinite plane to be rigorous. Obviously we are only able to measure over a finite area in practice, the near-field samples beyond this finite area being assumed to be zero. This assumption results in the introduction of a non-

[1] "Traditional" in this instance refers to a rectangular data area that is simply acquired from one end to the other by linear motion of the probe scanning in the vertical direction and stepping in the horizontal, or vice versa.

physical near-field discontinuity that in turn leads to a perturbation in the calculated far-field radiation pattern which is referred to as truncation uncertainty. If you have an antenna of a certain aperture area and you want to predict the far-zone pattern out to angle ξ off broadside, you need the near-field measurement area to be large enough in order to mitigate the impact of this truncation effect. In practice this translates into a widely used approximate rule (which has been established experimentally and derived theoretically) that is given in [3] as $L \geq W + P + 2H \tan \xi$. As sketched in Figure 1, dimension L is the distance of the PNF probe traverse, H is the separation between the AUT and probe, P is the probe aperture dimension, and W is the AUT aperture dimension. The predicted far-zone radiation pattern in this plane is considered unreliable beyond the "angle of validity". The rule gives us the minimum L required for a given angular region of interest. Although this rule is simple to evaluate and convenient, it only establishes a baseline measurement region and the impact of truncation is ultimately determined by the actual power level observed at the edge of the measurement plane.

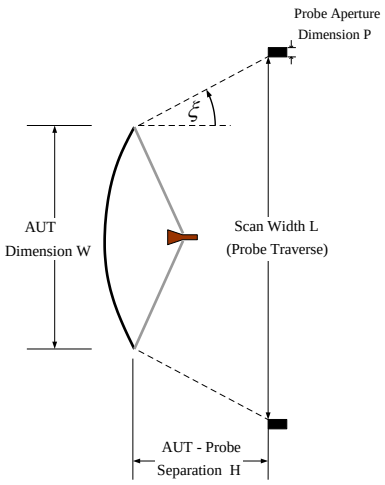

Figure 1 - Sketch showing the AUT aperture size and scan region dimensions.

A number of authors have proposed methods for reducing the truncation effect, principally to allow a larger AUT to be tested using a PNF facility of a given size. However, this would translate to test time reductions too, in that one would require fewer data points to be acquired. One method [4,5,6,7] employs integral equation techniques with the acquired near-field data used as a boundary condition to determine a set of equivalent currents over a plane between the PNF measurement plane and the AUT. The Fourier transform is then used on the equivalent currents to find the far-zone pattern of the AUT. The reliable region is found to be larger than it would have been had the original PNF data been used directly, reasons for which are provided in [5]. The additional computation that is needed to solve the integral equation for the equivalent currents can become prohibitive (even by present standards) when the AUT is electrically large, which is precisely the regime where PNF testing is most widely used. Although large reductions in the scan area are apparently possible, the method has not undergone exhaustive testing.

In another approach near-field data outside of the measurement area (but at points on the measurement plane) are estimated using an extrapolation algorithm on the available data that takes advantage of information on the AUT size [8]. This means one effectively has near-field data over a larger area than was actually measured. This near-field data can then be used in the conventional way to determine the far-zone fields. Because the near-field data occupies a larger measurement area the reliable far-field angular region is larger. This in turn means that for a specified angle of validity one can acquire data points over a smaller area than would normally be required, and determine the remaining data points through extrapolation. This would potentially lead to test time reduction. Unfortunately, in spite of the use of sophisticated regularization procedures to overcome the ill-conditioned nature of the process, "only a few samples outside of the measurement zone can be reliably recovered" [9]. In order to overcome such limitations the same authors devised a different method that uses the so-called sampling representation [10] that exploits known geometrical information about the AUT (namely its size, and thus the spatial bandwidth of its fields). It is not a mere extrapolation procedure, but uses the sampling theory to determine "how the information content of the field radiated by the AUT is distributed in the space around the AUT" [9]. It "recovers" the near-field values over the measurement plane beyond the region of measurement accessible by the PNF scanner, and is capable of eliminating truncation effects. However, the information needed to do so must be obtained by acquiring data through movement of the probe not only over the scan area on the conventional scan plane but also perpendicular to it. The method is effective, is not too computationally taxing, and could extend the applicability of a PNF scanner of limited size (in the x/y-plane over which the measurement is usually conducted) as long as it can move along the z-axis as well. Unfortunately such movement is often inconvenient and increases test times.

Instead of extrapolating the near-field data over the scan plane and then using it to find the far-zone fields, the technique described in [11], and references therein, extends the plane wave spectrum itself. The ill-conditioning of numerical processes that perform such tasks (and hence their susceptibility to noise) is circumvented by extending the plane wave spectrum

subject to a constraint that the equivalent source is concentrated in the AUT aperture (thereby utilizing known geometry information about the AUT). The particular numerical technique uses an iterative technique called the method of alternating projections, in particular a specific case thereof referred to as the Gerchberg-Papoulis algorithm. It starts by taking the original acquired data and finding the plane wave spectrum, which we know has a limited reliable region due to truncation of the scan area. This is then back-projected (inverse Fourier transform) to the AUT aperture plane. All points on the aperture plane that lie outside the AUT aperture are set to zero, and the plane wave spectrum then found from this constrained aperture distribution. This plane wave spectrum will have points outside the reliable region. These are retained. However, the new plane wave spectrum samples that lie in the original reliable region are replaced by their original starting values. These are then projected back to the aperture plane and the steps mentioned earlier repeated. And so on, iteratively, until some convergence criteria are met. Examples of such criteria are given in [11]. Although not specifically mentioned by the authors, it is known that the method of projections (no matter what it is used for) is susceptible to so-called traps and tunnels, and may not converge [12]. This would not be acceptable in an antenna measurement environment. Further testing of the method in [11] might reveal that this is not the case for this specific application, but with the limited two cases checked (one synthetic, the other experimental data) one cannot be certain of this. If indeed so, this could be an effective method for test time reduction, especially since the computing time is less than that of the integral equation methods.

The authors of [13] "investigate alternative sampling techniques that reduce the time required to collect the near-field data". The technique, "which reduces the number of sample points by 50%, makes use of the derivative theorem in Fourier transform theory" [13]. While conventional sampling theory requires one to sample the near-field data points at twice the highest spatial frequency, there is a more general sampling theorem that requires one to sample at only the highest spatial frequency if the near-field values plus their spatial derivatives are sampled at each point. There are a number of drawbacks with this approach. Firstly, the near-to-far-field transformation is more complicated, and a probe-compensation technique does not appear to have been devised for this approach. Secondly, and more importantly, suitable probes have not been developed for sampling the field derivatives.

These techniques collectively help us to understand the impact of PNF truncation and in some select cases reduce the impact of it. However, none of these techniques have gained widespread acceptance as a mainstream solution in industry. Also, a fundamental resistance to "computing additional measured data", irrespective of its theoretical correctness, will likely continue to limit the application of any single method in the short term. In the next section we propose two simple adaptive acquisition schemes that can be used to reduce test times to a minimum using only the near-field data acquired over the conventional scan region.

3.0 The Proposed Adaptive PNF Techniques

When considering traditional PNF acquisition a rectangular region of measurement is defined. The dimensions in x and y of this region is determined initially through application of the expression given in Section 2. The sequence of acquisition of these data samples is as depicted in Figure 2 and will be referred to as the "traditional method" below.

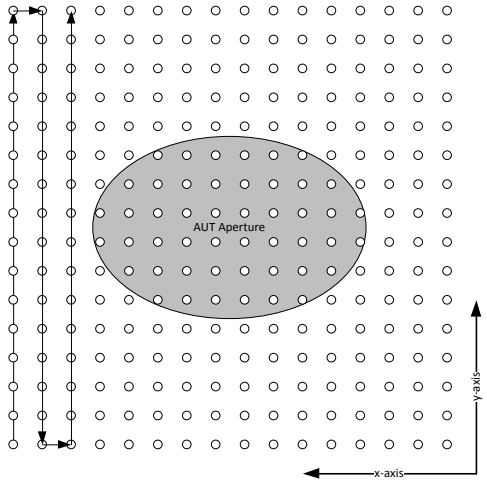

Figure 2 – A traditional rectangular PNF acquisition. Near-field grid points are shown superimposed on the AUT aperture (shaded), possible sampling points (o). Data is acquired by motion of the probe in the y-direction while stepping in the x-direction after completion of each y-cut.

The traditional method of acquisition typically requires mechanical and RF acquisition time, computation time and upon completion of these the desired far-field data can be evaluated. We recognize that the far-zone field computation time is very small compared to the data acquisition time and even if this computation is done repeatedly while the data is being acquired, it will not have any significant impact on total acquisition time. We therefore propose acquisition techniques that rely on far-field decision functions to impact near-field acquisition termination and regions of acquisition. This fact does not appear to have been previously exploited by others. The proposal is that such computations be used as part of an adaptive algorithm intent on reducing the amount of data

that has to be acquired, and hence the overall antenna testing time.

The first of these techniques is depicted in Figure 3. The probe moves on a rectangular spiral locus (as indicated), encompassing an increasingly larger number of sampling points as it moves. Acquisition starts at the center of the AUT aperture and progresses outward. Each spiral ring is regarded as an iteration in this instance and if we have a collection of sampled near-field values at the $(n-1)^{th}$ stage, as indicated by the locus (red) in Figure 3, we then let the probe continue along its data acquisition path until at the n^{th} stage we have an additional number of data points, as indicated by the locus (green) in Figure 3.

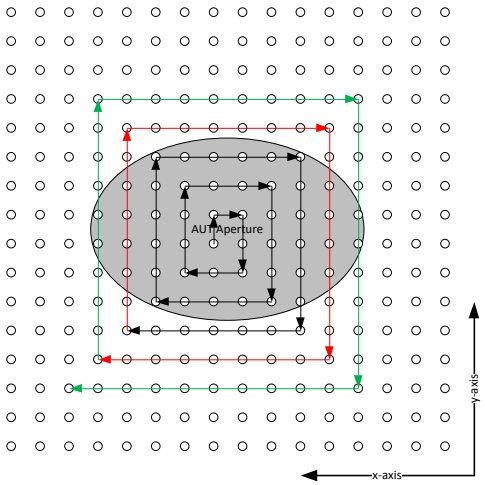

Figure 3 – Rectangular spiral PNF acquisition. Near-field grid points are shown superimposed on the AUT aperture (shaded), possible sampling points (o), and probe path history after $(n-1)^{th}$ (red) and n^{th} (green) iterations.

The second of the two acquisition techniques is depicted in Figure 4. The probe moves on a rectangular loop locus (as indicated), encompassing an increasingly larger number of sampling points as it moves away from the center of the AUT aperture. Each rectangular data ring is regarded as an iteration in this instance. At the end of the $(n-1)^{th}$ iteration the measured near-field power on each of the four sides of the loop are evaluated and the region of acquisition is expanded in the direction of the maximum power level by adding two rows or columns of data (dashed locus in Figure 4). After this additional acquisition the n^{th} iteration consists of a full rectangular data loop again and the process is repeated. The advantage of this acquisition is twofold. Firstly, the region of acquisition grows in the direction of higher near-field energy. This makes the method ideally suited for AUT aperture distributions that are elliptical or even asymmetric. Secondly, the method ensures that valid near-field data is being acquired during all scanner motion, thereby maximizing efficiency of the mechanical process.

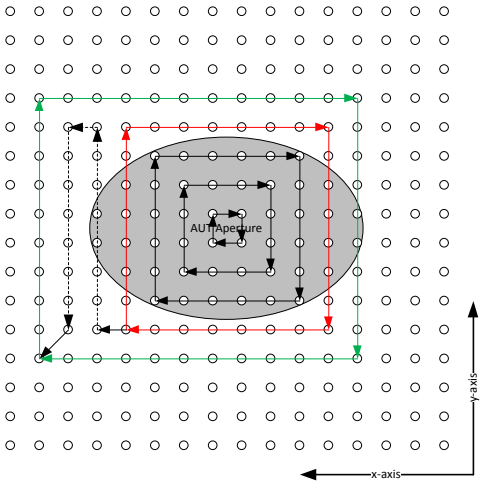

Figure 4 – Adaptive rectangular loop PNF acquisition scheme. Near-field grid points are shown superimposed on the AUT aperture (shaded), possible sampling points (o), and probe path history after $(n-1)^{th}$ (red) and n^{th} (green) iterations.

Although we have here indicated two specific probe loci, which are the ones examined in this paper, the method is equally applicable to other probe loci. At the end of each iteration we need to calculate a decision function value to decide whether to terminate the PNF data acquisition or not. If we can define such decision functions so that they provide a measure of the accuracy with which an identified performance index (e.g. directivity, side lobe level, cross-polarization level) is being determined at each iteration, then the PNF data acquisition can be terminated when the desired accuracy is reached. In this way we can acquire the smallest amount of data in order to achieve the desired accuracy of the selected performance measure of the AUT.

4.0 Experimental Investigation of Possible Decision Functions

A decision function must have a behavior that allows us to take an unambiguous decision that the PNF data acquisition may be terminated. Thus, decision functions should in some way be related to the performance measure(s) of interest in the particular application for which the PNF testing is being used. Preferably, the accuracy required for the said measure should also be known. The idea is that we reduce the near-field data acquisition time by requiring the minimum amount of near-field data necessary to achieve this by continually examining the value of the decision function while data acquisition is on-going. We will in the present section

discuss two kinds of decision functions. These will then be applied to PNF near-field data acquired for the different antennas whose information is summarized in Table 1.

Table 1 - Summary of AUT's test cases considered for decision function assessment

Antenna No.	Antenna Type	Antenna Size at Operating Frequency	Maximum Directivity (dBi)
1	Pyramidal Horn1	16λ x 16λ	21.1
2	Slotted Waveguide Array	23.5λ x 26.5λ	37.5
3	Offset Reflector	19.5λ x 23.0λ	37.1
4	Monopulse Reflector	23.5λ x 47.5λ	38.2

4.1 Normalized Pattern Differences Between Scan Iterations

After the n^{th} and $(n-1)^{th}$ scan iterations we denote the far-zone co-polarized electric field value in direction (θ_i, ϕ_j) by $E_{co}^{n}(\theta_i, \phi_j)$ and $E_{co}^{n-1}(\theta_i, \phi_j)$, respectively. The error term in direction (θ_i, ϕ_j) is, after the n^{th} iteration, then

$$f_{co}^{n}(\theta_i, \phi_j) = \frac{\left|E_{co}^{n}(\theta_i, \phi_j)\right| - \left|E_{co}^{n-1}(\theta_i, \phi_j)\right|}{\max_{i,j}\left\{\left|E_{co}^{n}(\theta_i, \phi_j)\right|\right\}} \qquad (1)$$

In other words, the error measure in each pattern direction is the difference between the normalized n^{th} and $(n-1)^{th}$ patterns in that direction. In all decision function work the full three-dimensional pattern is considered rather than just single pattern cuts. The normalization factor is simply the maximum field magnitude after the n^{th} iteration. Observe that the error term is direction dependent, that the values of the quantities in expression (1) are not in dB, and that a similar quantity can be defined for the cross-polarized fields. As an example, radiation pattern cuts of the slotted waveguide array, as well as the error pattern, after iterations n = 58 (dashed) and n = 59 (solid) are shown in Figure 5. If the normalized radiation pattern magnitude in direction (θ_i, ϕ_j) is E_{dB}, and we wish the uncertainty there to be $\pm\Delta_{dB}$, then we require

$$20\log\left|f_{co}^{n}(\theta_i, \phi_j)\right| \le E_{dB} + 20\log\left\{1 - 10^{-\Delta_{dB}/20}\right\} \qquad (2)$$

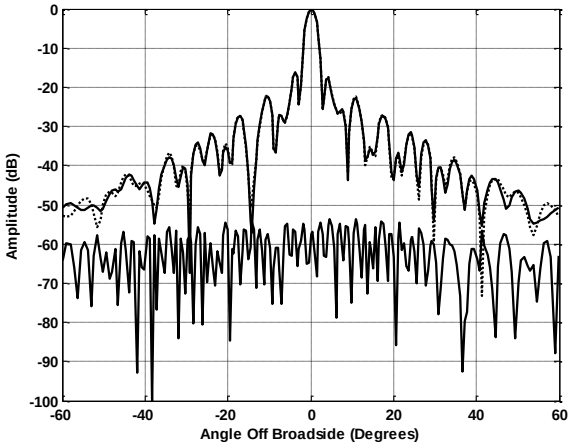

Figure 5 - Plot of the magnitude of $E_{co}^{n}(\theta,\phi)$ for n = 58 (dashed) and n = 59 (solid) as well as the error measure $f_{co}^{n}(\theta,\phi_o)$. Note that n = 58 means that the scan area consists of 58 by 58 samples.

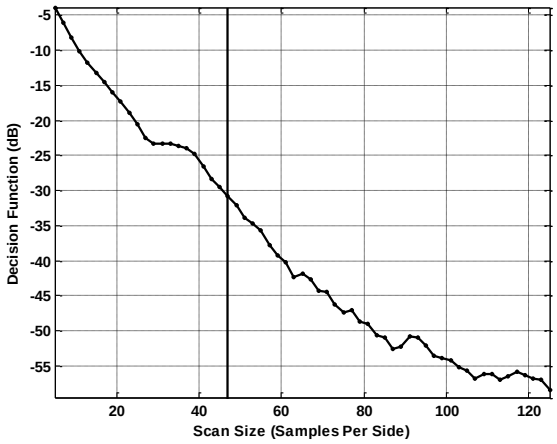

Figure 6 - Behavior of $\max_{i,j}\left|f_{co}^{n}(\theta_i,\phi_j)\right|$ as a function of scan size for the offset reflector for observation points lying within 30° of the broadside direction. The solid vertical line indicates the edge of the physical aperture of the AUT.

As a decision function we could also observe the value of f_{co}^{n} in some specific direction (θ_0, ϕ_0) or set of directions (such as those of the pattern maximum and important side lobes), or its maximum value in all planes out to some maximum angle, and continue scan iterations until these are sufficiently small. For example, Figure 6 shows $\max_{i,j}\left|f_{co}^{n}(\theta_i,\phi_j)\right|$ versus scan size for the offset reflector antenna for pattern directions lying within 30° of the

broadside direction. It drops below -50 dB for a scan size of about 83 samples per side. Since it is the largest value of the difference measure over the stated region of interest, it means that the uncertainty is better than ±0.5dB down to the -25dB pattern level and better than ±0.1dB down to the -10dB level.

4.2 Directivity Values

The co-polarized partial directivity in direction (θ,ϕ) can be computed from the plane wave spectrum using

$$D_{co}(\theta,\phi) = 4\pi\left|E_{co}(\theta,\phi)\right|^2 \Big/ 2\eta_o P_{rad}$$

where η_o is the free space intrinsic impedance and the total radiated power P_{rad} is found from the plane wave spectrum using [2, p. 115], with similar expressions for the cross-polarized case. We can observe the directivity in the direction of maximum radiation as the scan size increases. This is shown in Figure 7 for three of the antennas listed in Table 1, in both its co-polarized and cross-polarized forms. In the case of the co-polarized directivity this maximum occurs in the broadside direction, but in the cross-polarized case the direction in which the directivity is a maximum is not broadside. The locations of such maxima are easily determined through simple examination of the numerical data.

Both the co- and cross-polarized maximum directivity plots converge to some steady value as the scan size increases. At some point the directivity value changes negligibly from the nth to the (n-1)th scan. If this change is less than a certain amount, say the known accuracy within which the directivity can be determined by the measurement set-up, this can be used to terminate the PNF acquisition. We notice that for some of the antennas the co-polarized maximum directivity settles down at a smaller scan size than the cross-polarized one does. This is to be expected as the cross-polarized patterns are at much lower levels than the co-polarized ones, and are therefore more sensitive to truncation effects. If the polarisation properties are the important ones in some test then both the co- and cross-polarized directivities would need to be tracked. Instead of (or in addition to) the directivity maximum we could also observe the directivity in the direction of the highest side lobes.

Alternatively, we can directly track the changes in the directivity

$$\Delta D_{co}^{n}(\theta_0,\phi_0) = 10\log D_{co}^{n}(\theta_0,\phi_0) - 10\log D_{co}^{n-1}(\theta_0,\phi_0) \quad (4)$$

in a specific direction (θ_0,ϕ_0) say from one iteration to the next. The directivity differences are computed here by subtracting the dBi values of the directivity. The reason is that we want the value ΔD_{co}^{n} to decrease to zero as the scan size increases.

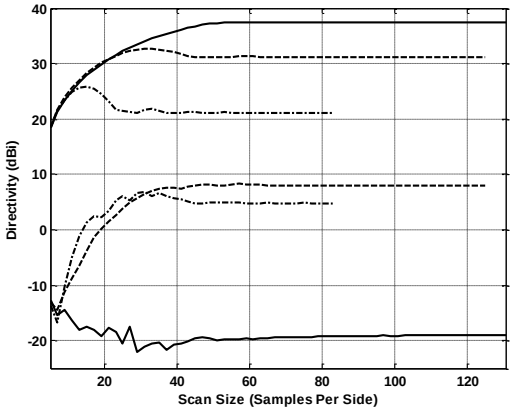

Figure 7 - Co-polarized and cross-polarized directivity, in the directions in which these quantities have their maxima, for the slotted waveguide array (—), offset reflector (----) and horn antenna 1 (-·-·-) as a function of increasing scan area. The lower curves are the cross-polarized cases.

Examples of $\Delta D_{co}^{n}(\theta_o,\phi_o)$ in the direction of maximum directivity (not the same as direction in which the directivity difference is a maximum) are shown in Figure 8 for the same AUTs whose maximum directivities are plotted in Figure 7. These all taper off as the scan size enlarges with increasing scan iteration count. The scanning can be terminated once $\Delta D_{co}^{n}(\theta_o,\phi_o)$ falls below 0.1dB, for instance. It is also possible to observe these differences in the directions of side lobes that might determine whether the AUT satisfies its pattern specifications.

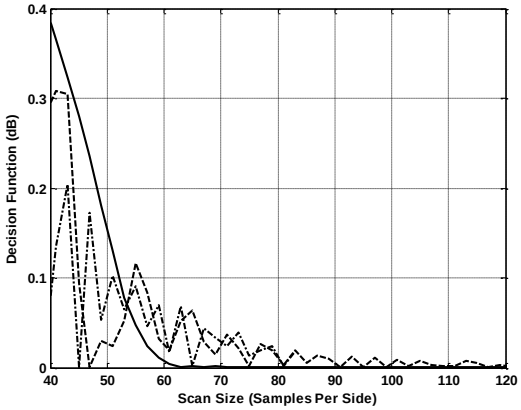

Figure 8 - Plots of the directivity differences in the direction of maximum directivity for the cases depicted in Figure 7; Slotted waveguide array (—), offset reflector (----) and horn antenna 1 (-·-·-).

5.0 Test Time Reduction Case Studies

Using the two adaptive acquisition techniques outlined in Section 3 (rectangular spiral locus & rectangular loop locus) seven different antenna test cases are considered. In all of these cases existing PNF data sets are in existence, acquired using the traditional acquisition method. Applying the two adaptive acquisition techniques in simulation is therefore feasible and potential test time reductions can be estimated. As seen in Section 4, test time will be dependent on the particular parameters of interest. For the purpose of this investigation we considered AUT directivity and first side lobe level as two distinct parameters.

Figure 9 shows the progression of AUT directivity for a Gregorian reflector test case considered. The blue curve represents the traditional acquisition case and clearly shows little convergence during the first half of the acquisition. Final convergence is achieved at roughly 75% of the full data set (showing that without using an adaptive acquisition technique, just an appropriate decision function to terminate acquisition would have potentially lead to a 25% reduction in test time). The red and green curves show the rectangular spiral and loop loci respectively. In this instance there is little advantage of the one over the other and they both display a potential 75% reduction of test time in terms of directivity. Through evaluation of equation (1) for all three test cases a resultant -60 dB error in the calculated directivity was confirmed at these respective acquisition termination points.

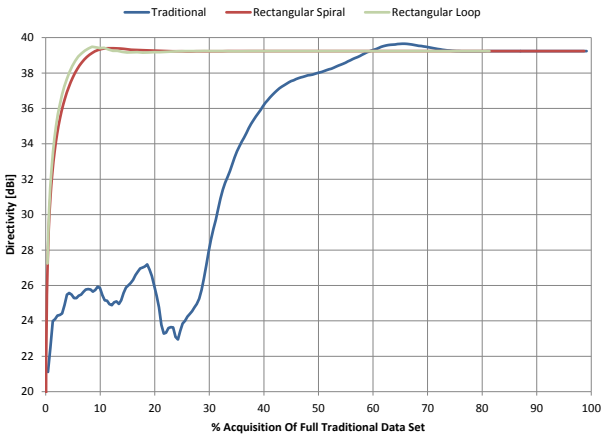

Figure 9 – Directivity value as a function of % acquisition for the Gregorian reflector test case. Traditional (blue), rectangular spiral locus (red) and rectangular loop locus (green) cases as shown.

Figure 10 shows the progression of the relative first side lobe level error for the Gregorian reflector test case considered. The blue curve represents the traditional acquisition case and appears to have converged during the first half of the acquisition. However, this is due to the fact that no data was acquired in the region of the side lobe during this stage. Significant error reduction is only observed beyond 60% of the full data set. The red and green curves again show the rectangular spiral and loop loci cases respectively. In this instance the rectangular spiral case displays a potential 70% reduction of test time and the rectangular loop case a potential 75% reduction of test time for the first side lobe. In all three instances a -60 dB error level was used as criterion.

Table 2 contains a summary of the seven test cases considered for assessing potential test time reduction using the two adaptive techniques when considering maximum directivity only. Table 3 contains the same information when considering the first side lobe of each AUT. Note that the test time reductions are with respect to the complete acquired data set and not with respect to the convergence point of the traditional acquisition method. This was done to illustrate the effect of the combined adaptive acquisition techniques with the termination decision functions. When applying the termination decision functions to the traditional acquisition method, test time reductions of between 20% and 40% are observed using the same measure against the full data set.

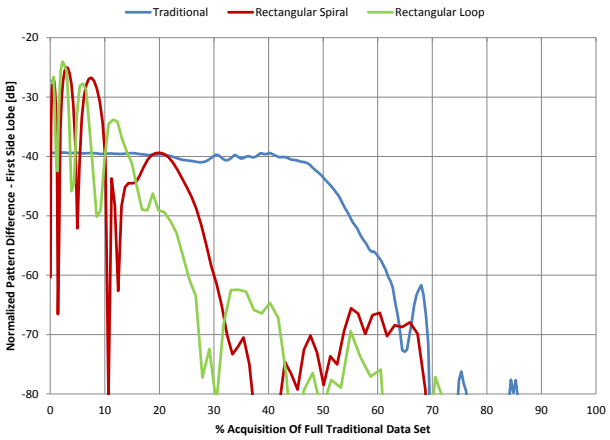

Figure 10 – Normalized pattern difference for first side lobe level as a function of % acquisition for the Gregorian reflector test case. Traditional (blue), rectangular spiral locus (red) and rectangular loop locus (green) cases as shown.

6.0 Conclusions

We have proposed the use of two simple adaptive acquisition techniques for PNF measurements. These techniques allow us to reduce test times by only proceeding with PNF data acquisition until the quantities being sought are within the accuracy we require. We have investigated several possible decision functions for use during the adaptive acquisition process.

Table 2 – Summary of AUT test cases considered for test time reduction – Directivity used as decision function. Test times are expressed as a percentage of traditional PNF acquisition time.

Antenna No.	Antenna Type	Rectangular Spiral Locus Test Time	Rectangular Loop Locus Test Time
1	Pyramidal Horn1	50%	50%
2	Slotted Waveguide Array	50%	50%
3	Offset Reflector	25%	20%
4	Monopulse Reflector	20%	20%
5	Pyramidal Horn2	40%	30%
6	Shaped beam reflector	55%	45%
7	Gregorian reflector	25%	25%

Table 3 – Summary of AUT test cases considered for test time reduction – First side lobe level normalized pattern difference used as decision function. Test times are expressed as a percentage of traditional PNF acquisition time.

Antenna No.	Antenna Type	Rectangular Spiral Locus Test Time	Rectangular Loop Locus Test Time
1	Pyramidal Horn1	70%	50%
2	Slotted Waveguide Array	35%	35%
3	Offset Reflector	55%	45%
4	Monopulse Reflector	20%	10%
5	Pyramidal Horn2	30%	25%
6	Shaped beam reflector	45%	32%
7	Gregorian reflector	30%	25%

The speed at which the far-zone field can be computed makes this computation feasible and therefore reduces the amount of data that has to be acquired by continuous monitoring of these decision functions. This is a relatively simple concept, but one that does not appear to have been proposed to date. It provides an uncomplicated way of reducing overall antenna test time, and can be accomplished with existing PNF scanning systems.

The two adaptive acquisition techniques proposed here represent a departure from the traditional PNF acquisition process in that it launches acquisition from the center of the AUT aperture. The region of highest energy is therefore acquired first and the near-field acquisition is adapted during the measurement process to ensure that regions of highest energy are included. The continual monitoring of the outlined decision functions allow for acquisition termination once a preset level of uncertainty has been achieved. The numerical data presented here shows that test time reductions of typically between 50% and 70% are possible over that currently achieved with traditional PNF acquisition methods.

7.0 REFERENCES

[1] P.D.T. O'Connor, Editorial, *IEEE Spectrum*, July 2001, pp.18

[2] S. Gregson, J. McCormick & C. Parini, *Principles of Planar Near-Field Antenna Measurements* (IET Electromagnetic Wave Series, 2007)

[3] A.C. Newell, "Error analysis techniques for planar near-field measurements", IEEE Trans. Antennas Propagat., Vol.36, No.6, p.754-768, June 1988.

[4] P. Petre & T.K. Sarkar, "Planar near-field to far-field transformation using an equivalent magnetic current approach", IEEE Trans. Antennas Propagat., Vol.40, No.11, p.1348-1356, Nov. 1992.

[5] P. Petre & T.K. Sarkar, "Differences between modal expansion and integral equation methods for planar near-field to far-field transformation", Progress in Electromagnetics Research (*PIER 12*), pp.37-56, 1996.

[6] J.R. Pérez & J. Basterrechea, "Antenna far-fields from planar acquisition using micro-genetic algorithms", Electron. Lett., Vol.39, No.13, p.948-949, June 2003.

[7] Y. Álvarez, F. Las-Heras and M.R. Pino, "Reconstruction of Equivalent Currents Distribution Over Arbitrary Three-Dimensional Surfaces Based on Integral Equation Algorithms", IEEE Trans. Antennas Propagat., Vol.55, No.12, pp.3460-3468, Dec.2007.

[8] O.M. Bucci, G. D'Elia & M.D. Migliore, "A new strategy to reduce the truncation error in near-field/far-field transformations", Radio Science, Vol.35, No.1, pp.3-18, January-February 2000.

[9] O.M. Bucci & M.D. Migliore, "A new method for avoiding the truncation error in near-field antennas measurements", IEEE Transactions on Antennas & Propagation, Vol.54, No.10, pp.2940-2952, Oct.2006.

[10] O.M. Bucci, C. Gennarelli & C. Savaresse, "Representation of electromagnetic fields over arbitrary surfaces by a finite and nonredundant number of samples", IEEE Trans. Antennas Propagat., Vol.46, pp.351-359, 1998.

[11] E. Martini, O. Breinbjerg & S. Maci, "Reduction of truncation errors in planar near-field aperture antenna measurements using the Gerchberg-Papoulis algorithm", IEEE Trans. Antennas Propagat., Vol.56, No.11, pp.3485-3493, Nov.2008.

[12] H. Stark & Y. Yang, *Vector Space Projections: A Numerical Approach to Signal and Image Processing, Neural Nets, And Optics* (Wiley, 1998)

[13] L.E. Corey & D.R. O'Neil, "Differential sampling of planar near-fields", *IEEE AP-S Symp. Digest*, pp.191-194, June 1986.